

Quantum squeezing and sensing with pseudo anti-parity-time symmetry

Xi-Wang Luo,¹ Chuanwei Zhang,^{1,*} and Shengwang Du^{1,†}

¹*Department of Physics, The University of Texas at Dallas, Richardson, Texas 75080-3021, USA*

The emergence of parity-time (\mathcal{PT}) symmetry has greatly enriched our study of symmetry-enabled non-Hermitian physics, but the realization of quantum \mathcal{PT} -symmetry faces an intrinsic issue of unavoidable symmetry-breaking Langevin noises. Here we construct a quantum pseudo-anti- \mathcal{PT} (pseudo- \mathcal{APT}) symmetry in a two-mode bosonic system without involving Langevin noises. We show that the pseudo- \mathcal{APT} phase transition across the exceptional point yields a transition between different types of quantum squeezing behaviors, *i.e.*, the squeezing factor increases exponentially (oscillates periodically) with time in the pseudo- \mathcal{APT} symmetric (broken) region. Such dramatic changes of squeezing factors and associated quantum states near the exceptional point are utilized for ultra-precision quantum sensing with divergent sensitivity. These exotic quantum phenomena and sensing applications induced by quantum pseudo- \mathcal{APT} symmetry can be experimentally observed in two physical systems: spontaneous wave mixing nonlinear optics and atomic Bose-Einstein condensates.

Introduction.—Hermiticity and real eigenvalues of a Hamiltonian are key postulates of quantum mechanics. While non-Hermitian Hamiltonians emerged from the interaction with external environments generally possess complex eigenspectra, they can exhibit entirely real eigenvalues in the presence of parity-time (\mathcal{PT}) symmetry [1–7]. When the non-Hermiticity parameter exceeds a critical value, known as the exceptional point (EP), the \mathcal{PT} -symmetry can be spontaneously broken for the eigenstates, leading to a phase transition from the \mathcal{PT} -symmetric phase with purely real eigenvalues to the \mathcal{PT} -broken phase with complex conjugate eigenvalue pairs. Such \mathcal{PT} phase transition showcases both fundamentally new physics and technologically important applications [8–20] that may not be available in Hermitian systems. In the past decade, significant experimental and theoretical progress has been made for exploring \mathcal{PT} -symmetry physics in various physical systems (e.g., photonics, acoustics, ultracold atoms, etc.), which generally utilize the control of gain/loss in classical wave systems. However, an intrinsic issue for studying \mathcal{PT} -symmetry physics in the quantum realm [21–26] is that a \mathcal{PT} -symmetric Hamiltonian involving gain/loss does not preserve the commutation relationships of quantum operators, therefore Langevin noises, which break \mathcal{PT} symmetry, must be included in quantum systems [27]. Two recent experimental approaches to circumvent this issue for quantum \mathcal{PT} symmetry include discarding quantum noise through post-selection measurement [24] and Hamiltonian dilation through embedding a non-Hermitian Hamiltonian into a larger Hermitian system [25].

Anti- \mathcal{PT} (\mathcal{APT}) represents another non-Hermitian symmetry with the Hamiltonian anticommuting with \mathcal{PT} operator and has recently attracted great interests [28–35]. Recent studies showed that an \mathcal{APT} -symmetric system does not have to involve gain/loss [35, 36] of classical fields, making it possible to realize a quantum \mathcal{APT} -symmetry without Langevin noises. In this Letter,

we construct a quantum \mathcal{APT} -symmetry in a two-mode bosonic system, where the dynamical Hamiltonian matrix is non-Hermitian and preserves the \mathcal{APT} -symmetry, while the second-quantized Hamiltonian is Hermitian. In this sense, we call it a pseudo- \mathcal{APT} symmetry. Our main results are:

i) The quantum pseudo- \mathcal{APT} -symmetry builds on coupling Bose creation operator of one field with the annihilation operator of the other field, yielding the Hermiticity of the second-quantized Hamiltonian that does not require Langevin noises. Nevertheless, the pseudo- \mathcal{APT} Hamiltonian matrix still possesses the transition between real and complex eigenvalues and EP. In the classical limit, the Bose field operators are replaced by complex numbers, and the model reduces to conventional non-Hermitian physics with the \mathcal{APT} symmetry [35, 36].

ii) The phase transition across the EP with the pseudo- \mathcal{APT} symmetry yields a transition between different types of quantum squeezing behaviors. Specifically, the two-mode squeezing factor oscillates periodically with time in the pseudo- \mathcal{APT} -broken region, increases linearly at EP, and grows exponentially in the pseudo- \mathcal{APT} -symmetric region. Optical field squeezed states have been widely studied because of their fundamental interest (e.g., the implementation of EPR paradox) as well as broad applications in quantum information processing (e.g., continuous-variable quantum teleportation) and quantum metrology (e.g., gravitational wave detection) [37, 38]. Here the connection between pseudo- \mathcal{APT} phase transition and the transition of quantum squeezed states is established for the first time.

iii) The dramatic changes of quantum squeezing factors and states close to the EP make them ultra-sensitive to some parameters, thus can be utilized to achieve ultra-precision quantum sensing. We show that simple measurement schemes can reach the sensitivity close to the quantum Cramér-Rao bound given by the quantum Fisher information [39, 40], which exhibits divergent feature as the EP is approached.

iv) We propose that the connection between the quantum pseudo- \mathcal{APT} symmetry and the transition of squeezed states as well as the ultra-precision quantum sensors can be realized experimentally in spontaneous wave mixing nonlinear optics and ultracold atomic Bose-Einstein condensates (BEC). In the later BEC case, we also establish the connection between the pseudo- \mathcal{APT} -driven phase transition and the well-known transition to dynamical instability.

Pseudo- \mathcal{APT} -symmetry and quantum squeezing.— Consider a two-mode bosonic model described by the dynamical equation

$$i\partial_t (\hat{a}_1, \hat{a}_2^\dagger)^T = H (\hat{a}_1, \hat{a}_2^\dagger)^T, \quad (1)$$

where \hat{a}_j and \hat{a}_j^\dagger are the bosonic annihilation and creation operators. The non-Hermitian dynamical Hamiltonian matrix

$$H = \delta\sigma_z + i\kappa\sigma_x = \begin{pmatrix} \delta & i\kappa \\ i\kappa & -\delta \end{pmatrix}, \quad (2)$$

where the detuning δ and coupling coefficient κ are both real numbers. H satisfies $\{\mathcal{PT}, H\} = 0$, with the parity operator $\mathcal{P} = \sigma_x$ and the time-reversal complex conjugate operator \mathcal{T} . The EP occurs at $|\kappa| = |\delta|$ (the signs of δ and κ are unimportant). In the classical limit, the field operators \hat{a}_1 and \hat{a}_2^\dagger are replaced by complex numbers, and the model reduces to the non-Hermitian system with \mathcal{APT} symmetry [35, 36]. In the quantum realm, although the dynamics are governed by a non-Hermitian matrix H preserving \mathcal{APT} symmetry, the corresponding second-quantized Hamiltonian $\mathcal{H} = \delta(\hat{a}_1^\dagger\hat{a}_1 + \hat{a}_2^\dagger\hat{a}_2) + i\kappa(\hat{a}_1^\dagger\hat{a}_2^\dagger - \hat{a}_1\hat{a}_2)$ is Hermitian. In this sense, we call it a pseudo- \mathcal{APT} symmetry.

In the pseudo- \mathcal{APT} -symmetric region (*i.e.*, the eigenstates of H are \mathcal{PT} -symmetric) $|\delta| < |\kappa|$, H has imaginary eigenvalues $\lambda_\pm = \pm i\lambda_0$ with $\lambda_0 = \sqrt{|\kappa^2 - \delta^2|}$ (λ_0 vanishes at the EP $|\kappa| = |\delta|$). While in the pseudo \mathcal{APT} -broken region $|\delta| > |\kappa|$, H has real eigenvalues $\lambda_\pm = \pm\lambda_0$. The field operators at time t can be obtained as [41]

$$\hat{a}_j(t) = A\hat{a}_j(0) + B\hat{a}_{\bar{j}}^\dagger(0), \quad (3)$$

where \bar{j} represents the different mode number from j . In the pseudo- \mathcal{APT} -broken (symmetric) region, we have $A = \cos(\lambda_0 t) - i\frac{\delta}{\lambda_0} \sin(\lambda_0 t)$ ($A = \cosh(\lambda_0 t) - i\frac{\delta}{\lambda_0} \sinh(\lambda_0 t)$) and $B = \frac{\kappa}{\lambda_0} \sin(\lambda_0 t)$ ($B = \frac{\kappa}{\lambda_0} \sinh(\lambda_0 t)$). $|A|^2 - |B|^2 = 1$ in both regions and the bosonic commutation relations $[\hat{a}_j(t), \hat{a}_{j'}^\dagger(t)] = [\hat{a}_j(0), \hat{a}_{j'}^\dagger(0)] = \delta_{jj'}$ are preserved without Langevin noises.

The quantum squeezing can be characterized by the quadrature operators $\hat{X}_j(\varphi, t) = [e^{-i\varphi}\hat{a}_j(t) + h.c.]/2$ of the two modes, which satisfy $\hat{X}_1(\varphi_+, t) \pm \hat{X}_2(\varphi_+, t) = S^{\pm 1}[\hat{X}_1(\varphi_-, 0) \pm \hat{X}_2(\varphi_-, 0)]$. Here $A = A_0 e^{i\varphi_A}$ and $B = B_0 e^{i\varphi_B}$ with the positive amplitudes $A_0^2 - B_0^2 = 1$,

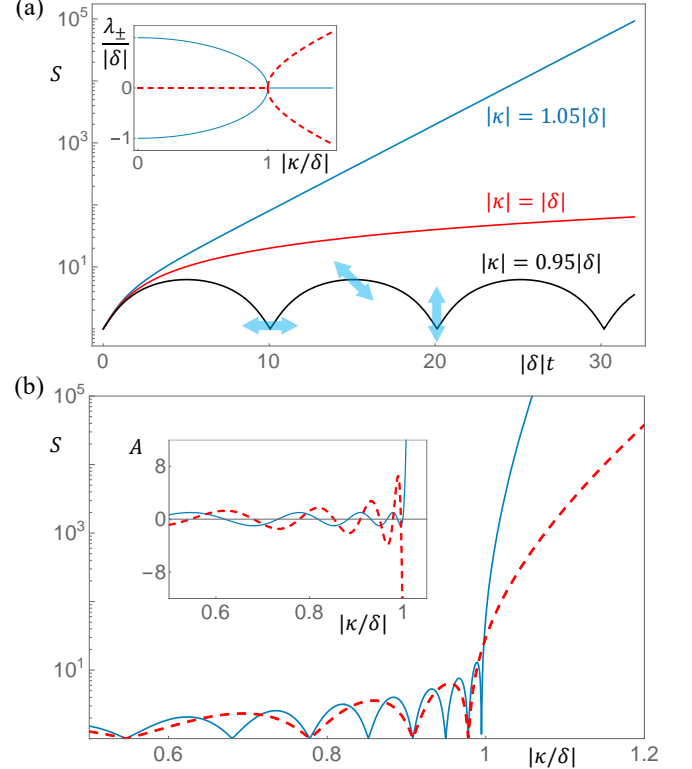


FIG. 1: The relation between quantum squeezing and pseudo- \mathcal{APT} symmetry. (a) The squeezing factor versus evolution time for different κ . $|\kappa/\delta| = 0.95, 1$ and 1.05 correspond to pseudo- \mathcal{APT} broken, EP and pseudo- \mathcal{APT} symmetric regions, respectively. Blue arrows indicate the two-mode squeezing directions for $\kappa, \delta > 0$. The inset shows the eigenvalues of H . Solid (dashed) lines are the real (imaginary) parts. (b) Squeezing factor versus κ for different evolution time. Solid (dashed) line corresponds to $|\delta|t = 30$ ($|\delta|t = 15$). Inset shows A versus $|\kappa/\delta|$ with $\delta t = 30$. Solid (dashed) line is the real (imaginary) part. $B = -\kappa \text{Im}[A]/\delta$.

$S = A_0 + B_0 \geq 1$ is the two-mode squeezing factor, $\varphi_+ = (\varphi_B + \varphi_A)/2$ is the squeezing angle. The angle $\varphi_- = (\varphi_B - \varphi_A)/2$ is not important because the initial state is usually unentangled and isotropic (*e.g.* the vacuum or coherent state). In the pseudo- \mathcal{APT} -symmetric region, one of the eigenmodes disappears after a long time evolution due to the imaginary eigenvalues, therefore $A_0 \simeq B_0 \simeq \frac{\kappa}{2\lambda_0} e^{\lambda_0 t}$ and the squeezing factor $S \simeq \frac{\kappa}{\lambda_0} e^{\lambda_0 t}$ grows exponentially. In the pseudo- \mathcal{APT} -broken region, both eigenvalues are real and $S \leq \sqrt{(|\delta| + |\kappa|)/(|\delta| - |\kappa|)}$.

Fig. 1 shows the transition between different types of quantum squeezing behaviors with the pseudo- \mathcal{APT} symmetry. In the pseudo- \mathcal{APT} -symmetric region ($|\kappa/\delta| > 1$), the squeezing factor S increases monotonically due to purely imaginary λ_\pm , and the increase becomes exponential at the long time. The squeezing angle ϕ_+ quickly changes from $\frac{1}{2}\text{Arg}[\kappa]$ to its saturated value $\frac{1}{2}\text{Arg}[\kappa\lambda_0 - i\kappa\delta]$. In the pseudo- \mathcal{APT} -broken region, S

shows oscillation behavior with a period $T = \pi/\lambda_0$, going back to 1 (non-squeezing) at $t = nT$ and reaching the maximum $\sqrt{(|\delta| + |\kappa|)/(|\delta| - |\kappa|)}$ at $t = (n + 1/2)T$ (n is an integer). In each period starting from $S = 1$, φ_+ changes from $\frac{1}{2}\text{Arg}[\kappa]$ to $\text{Arg}[-i\kappa\delta]$ as S increases to the maximum, and then to $\frac{1}{2}\text{Arg}[-\kappa]$ as S decreases to 1, as schematically illustrated in Fig. 1a. At the EP, two eigenmodes coalesce to a single mode. We have $A = 1 - i\delta t$, $B = \kappa t$ [41], and $S = \sqrt{1 + \delta^2 t^2} + |\kappa|t$ increases linearly at long time $|\delta|t \gg 1$. φ_+ changes monotonically from $\frac{1}{2}\text{Arg}[\kappa]$ to $\frac{1}{2}\text{Arg}[-i\kappa\delta]$. The results at the EP are consistent with the $|\kappa| \rightarrow |\delta|$ limit from both sides.

Since the squeezing behavior changes dramatically across the EP, the quantum state for a given time should also be sensitive to the system parameters δ, κ around the EP. In Fig. 1b, we plot the squeezing factor as a function of $|\kappa/\delta|$ at different times. We see S oscillates with increasing amplitude and frequency as $|\kappa|$ increases to the EP. Near the EP, the squeezing factor (thereby the quantum state) exhibits a sharp change around $S = 1$ (i.e., for κ satisfying $\lambda_0 t = n\pi$), where the system returns to its initial non-squeezing quantum state. The coefficients A and B of the quantum state show similar oscillation behaviors as S (the inset of Fig. 1b). Such critical behavior around the EP can be utilized to implement ultra-precision quantum sensing.

Quantum sensing.—Precision measurements are long pursued due to their vital importance in physics and many other sciences. Quantum sensing, such as quantum entanglement [39, 40] and phase-transition criticality based sensors [42–47], utilize unique quantum phenomena for ultra-precision measurements. Recent studies showed that the EPs of the \mathcal{PT} symmetry can enhance the optical sensing in the classical region [48]. Here we explore ultra-precision quantum sensing enabled by the quantum pseudo- \mathcal{APT} -symmetry without quantum noises.

We focus on the pseudo- \mathcal{APT} -broken region $|\kappa| < |\delta|$, which is dynamical stable without the exponential increase of excitations. We propose a simple scheme to measure A and B directly, which are sensitive to the system parameters κ, δ . The sensor precision is at the same order as quantum Cramér-Rao bound set by the quantum Fisher information of the quantum state, which shows divergent feature close to the EP.

We consider a coherent initial state $|\psi_0\rangle = |\alpha_1, \alpha_2\rangle$ of two bosonic modes for the quantum sensor, and the results for different initial states are similar. After an evolution time t , we perform the quadrature measurements $\hat{X}_j(0, t)$ using standard homodyne detection. The mean value and variance of $\hat{X}_j(0, t)$ can be obtained as

$$\langle \hat{X}_j(0, t) \rangle_{\psi_0} = \text{Re}[A\alpha_j + B\alpha_j^*] \quad (4)$$

$$[\Delta \hat{X}_j(0, t)]^2 = \frac{1}{4}(A_0^2 + B_0^2), \quad (5)$$

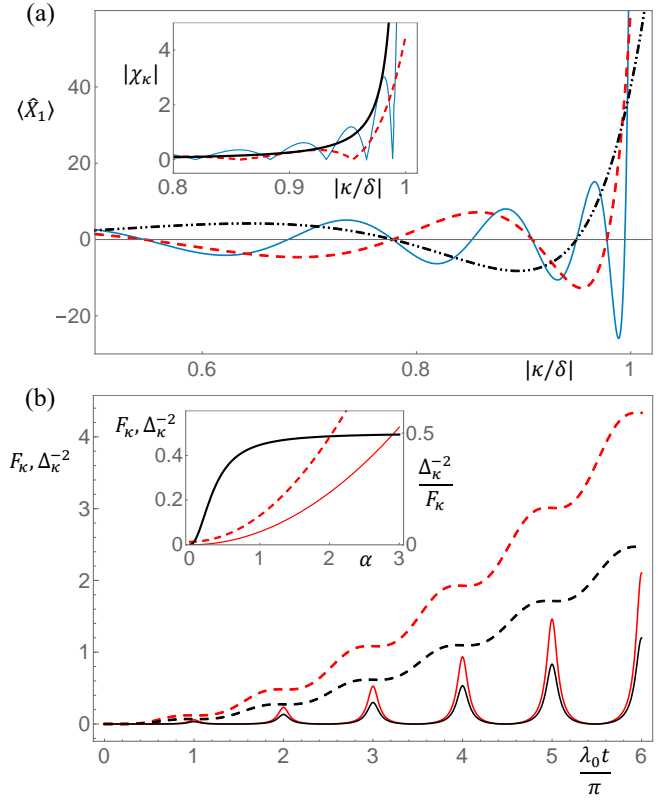


FIG. 2: Quantum sensing based on pseudo- \mathcal{APT} symmetry. (a) The quadrature $\langle \hat{X}_1 \rangle$ versus κ at different evolution time, with $\alpha = 2 \cdot \text{sign}(\delta)$. $|\delta|t = 10, 15$ and 30 are shown by the dash-dotted, dashed and solid lines, respectively. Inset shows the corresponding susceptibility $|\chi_\kappa|$ (in unit of 10^3), with bold solid line showing the results with κ -dependent time satisfying $\lambda_0 t = 2\pi$. The working points are located near $\langle \hat{X}_1 \rangle = 0$ (i.e., the maxima of χ_κ). (b) The inverse variance Δ_κ^{-2} (solid lines) of the observable and the quantum Fisher information F_κ (dashed lines) as functions of evolution times (in unit of 10^7) with $\alpha = 2$. Red and black lines are for $\kappa/\delta = 0.95$ and 0.94 , respectively. Local maxima of Δ_κ^{-2} give the work points $\lambda_0 t = n\pi$. Inset shows the results as functions of α for $\lambda_0 t = 2\pi$ and $\kappa/\delta = 0.95$, with bold black line corresponding to $\Delta_\kappa^{-2}/F_\kappa$.

with $\bar{j} \neq j$. Without loss of generality, we choose $\kappa\delta > 0$ and set $\alpha_2 = -i\alpha_1 \equiv \alpha$ (different choices of parameters generally would not affect the sensing precision). The observable $\langle \hat{X}_1(0, t) \rangle_{\psi_0}$ reads $\langle \hat{X}_1(0, t) \rangle_{\psi_0} = \alpha \sin(\lambda_0 t) \frac{\kappa + \delta}{\lambda_0}$. In Fig. 2a, we plot $\langle \hat{X}_1(0, t) \rangle_{\psi_0}$ as a function of κ with fixed δ and t , which possesses strong and fast oscillation close to the EP. Such oscillation becomes more pronounced as the evolution time increases.

The measurement of the change of $\langle \hat{X}_j(0, t) \rangle_{\psi_0}$ with κ gives the susceptibility $\chi_\kappa(t) \equiv \partial_\kappa \langle \hat{X}_1(0, t) \rangle_{\psi_0} = -\alpha \cos(\lambda_0 t) \frac{\kappa(\kappa + \delta)t}{\lambda_0^2} + \alpha \sin(\lambda_0 t) \frac{\kappa(\kappa + \delta)}{\lambda_0^3} + \alpha \sin(\lambda_0 t) \frac{1}{\lambda_0}$, which exhibits divergent feature close to the EP $\kappa \rightarrow \delta$ (i.e., $\lambda_0 \rightarrow 0$). Similar results apply to the susceptibility with δ . In Fig. 2a, we plot χ_κ for a fixed evolution

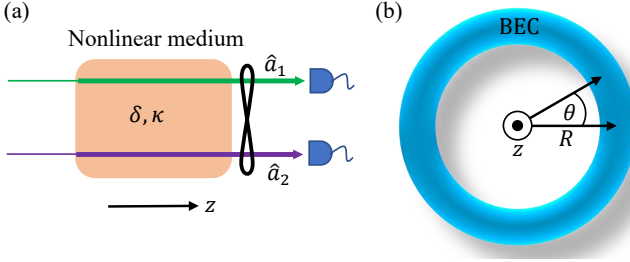


FIG. 3: Experimental implementations. (a) Schematic optical setup for realizing the model in Eq. 1. (b) Experimental realization based on cold atomic BEC in a ring trap.

time as well as a κ -dependent evolution time satisfying $t = nT = n\pi/\lambda_0$. The later one possesses a divergent scaling $\chi_\kappa(nT) = -\alpha \frac{\kappa(\kappa+\delta)n\pi}{\lambda_0^3} \sim \lambda_0^{-3}$. Longer evolution time is required for smaller λ_0 to observe such divergence.

The precision of the parameter estimation is given by the variance $\Delta_\kappa^2 = [\Delta \hat{X}_1]^2/\chi_\kappa^2$, and the performance of the sensing scheme can be evaluated by comparing the inverse variance Δ_κ^{-2} with the quantum Fisher information F_κ , whose inverse gives the ultimate precision for quantum sensing, i.e., reaching quantum Cramér-Rao bound $\Delta_\kappa^{-2} \leq F_\kappa$ (optimal measurement is usually required). For the coherent initial state $|\psi_0\rangle$,

$$F_\kappa(t) = 4A_0^4 |\partial_\kappa \frac{B}{A^*}|^2 + 4(A_0^2 + B_0^2) \sum_j |\partial_\kappa \langle \hat{a}_j(t) \rangle_{\psi_0}|^2 - 16\Re[A^* B^* \partial_\kappa \langle \hat{a}_1(t) \rangle_{\psi_0} \partial_\kappa \langle \hat{a}_2(t) \rangle_{\psi_0}] \quad (6)$$

after the evolution time t [41]. In Fig. 2b, we compare Δ_κ^{-2} with F_κ at different evolution times. We see that Δ_κ^{-2} has some narrow peaks when κ satisfies $t = n\pi/\lambda_0$ (i.e., the precision Δ_κ reaches the minimum) for fixed δ and $|\kappa| \lesssim |\delta|$, while $F_\kappa(t)$ smoothly increases with κ and takes larger values for all κ near the EP. At working points $t = n\pi/\lambda_0$, $F_\kappa(nT) = \left[8 + \frac{4\kappa^2}{\alpha^2(\kappa+\delta)^2}\right] \chi_\kappa^2 \sim \lambda_0^{-6}$, while $\Delta_\kappa^{-2}(nT) = 4\chi_\kappa^2 \simeq 0.5F_\kappa$ for coherent amplitudes α that are not too weak (e.g., $\alpha \sim 2$), as shown in Fig. 2b.

Notice that the squeezing factor $S = 1$ at the working points, therefore the ultra-precision sensitivity mainly originates from the pseudo- \mathcal{APT} symmetry breaking rather than the squeezing itself or entanglement. The eigenvalues of H have square-root splitting $\lambda_0 = \sqrt{\delta^2 - \kappa^2}$ with divergent sensitivity $\partial_\kappa \lambda_0 = -\frac{\kappa}{\lambda_0}$ close to the EP. In addition, the eigenmodes are not orthogonal and coalesce at the EP, which are responsible for the factor λ_0^{-1} in the final Bosonic field $\hat{a}_j(t)$. Together they gives the divergent scaling λ_0^{-3} in the susceptibility $\chi_\kappa(t)$ for the evolution time $t \sim \lambda_0^{-1}$. During the evolution, the number of Bosonic excitations $N \sim \lambda_0^{-2}$, therefore $\Delta_\kappa^{-2} \sim N^2 t^2$, which is the same order as the Heisenberg limit.

Experimental realization.—The quantum pseudo- \mathcal{APT} symmetry physics can be realized in quantum optics sys-

tems or atomic BECs. In the quantum optical implementation, we can utilize nonlinear wave mixing such as spontaneous parametric down conversion (SPDC) [49, 50] and spontaneous four-wave mixing (SFWM) [51, 52] with carefully designed parameters. In SPDC, a single pump laser beam is used to dress the nonlinear medium. In SFWM, two pump laser fields are used, which provide more degrees of freedom to system control. In both cases, two quantum modes ($\hat{a}_{1,2}$) copropagate along the z direction in the nonlinear optical medium and are coupled through a nonlinear coupling coefficient κ which can be tuned by changing the pump laser(s) intensity and frequency, as well as the material properties. The parameter δ is associated with the phase mismatching $\delta = -\Delta k/2$, where $\Delta k = (\mathbf{k}_1 + \mathbf{k}_2 - \sum \mathbf{k}_{\text{pump}}) \cdot \hat{\mathbf{z}}$ with \mathbf{k}_j being the wave vectors and $\hat{\mathbf{z}}$ the unit vector. In this system, the propagation along the z direction simulates the time evolution in our theoretical model (i.e., $t = z$). Different from previous studies in the classical optics regime that require seeding at least one mode [35, 36], here both quantum modes can initially start from vacuum fluctuations. A schematic illustration of the optical setup is shown in Fig. 3a and more detailed studies are provided in the supplementary materials [41].

In the atomic implementation, we consider a BEC in a ring dipole trap (as shown in Fig. 3b) with strong confinement along z and radial directions, which can be realized by Laguerre-Gaussian lasers as demonstrated in recent experiments [53, 54]. The dynamics are reduced to one dimension (i.e., the azimuthal angle θ). We can expand the BEC field operator in the angular momentum space as [55, 56]

$$\Psi(\theta, t) = e^{-i\mu t - i\pi/4} \Phi(t) + e^{-i\mu t} \sum_{n \neq 0} \hat{\psi}_n(t) \frac{e^{in\theta}}{\sqrt{2\pi}}, \quad (7)$$

where Φ is the condensate wave function (Φ is real initially and $\pi/4$ is a gauge choice), $\mu = -g|\Phi|^2 - g \sum_n \langle \psi_n^\dagger \psi_n \rangle / 2\pi$ is the chemical potential, and g is the interaction strength ($g > 0$ corresponds to attractive interaction). The quantum excitation operators $\hat{\psi}_n(t)$ satisfy the Bogoliubov equation [41]

$$i\partial_t \begin{pmatrix} \hat{\psi}_n \\ \hat{\psi}_{-n}^\dagger \end{pmatrix} = \begin{pmatrix} \delta_n & i\kappa \\ i\kappa^* & -\delta_n \end{pmatrix} \begin{pmatrix} \hat{\psi}_n \\ \hat{\psi}_{-n}^\dagger \end{pmatrix}, \quad (8)$$

which shares the same form as Eq. 1. Here $\delta_n = n^2 E_1 - g|\Phi|^2$, $\kappa = g\Phi^2$, and $E_1 = \frac{1}{2mR^2}$ is the kinetic energy of the first excited state along the ring with radius R . At $g = 0$, the quantum pseudo- \mathcal{APT} symmetry is broken for all n . As g increases, the BEC becomes dynamical unstable when $2g|\Phi|^2 > E_1$ (i.e., $|\kappa| > |\delta_1|$), where the pseudo- \mathcal{APT} symmetry is restored for $n = 1$, and the excitation number and squeezing factor grow exponentially [57, 58]. For the quantum sensing, we can first prepare the BEC to its ground state with $g \simeq 0$.

The initial coherent state for $n = \pm 1$ can be generated by Raman process with Laguerre-Gaussian beams carrying ± 1 orbital angular momentum. Then we increase g to the working point near the EP (*i.e.*, $2g|\Phi|^2 = E_1$). The quadratures \hat{X}_n , which is proportional to the visibility of the density modulation along θ , can be measured by density imaging. The performance of the sensor is very similar as that shown in Fig. 2 (see [41] for more details).

Conclusion and discussion.—In summary, we construct a quantum pseudo- \mathcal{APT} symmetry without Langevin noises and show that its phase transition across EP yields a dramatic transition of quantum squeezed states. The divergent sensitivity of squeezed states close to the EP can be utilized for ultra-precision sensing approaching the quantum limit. The experimental realization of such quantum pseudo- \mathcal{APT} symmetry in nonlinear quantum optical wave mixing and ultracold atomic BEC provide realistic platforms for studying quantum non-Hermitian physics and its quantum sensing applications. The two-mode quantum pseudo- \mathcal{APT} symmetry can also be generalized to a multi-mode system supporting higher-order EPs [59, 60], which may lead to novel symmetry breaking physics and even higher sensing precision.

Acknowledgments.—X.W.L. and C.Z. acknowledge support from NSF (PHY-2110212), ARO (W911NF17-1-0128), and AFOSR (FA9550-20-1-0220). S.D. acknowledges the Texas STARs and Start-Up fundings from The University of Texas at Dallas.

* Electronic address: Chuanwei.Zhang@utdallas.edu

† Electronic address: dusw@utdallas.edu

[1] C. M. Bender and S. Boettcher, Real Spectra in Non-Hermitian Hamiltonians Having \mathcal{PT} Symmetry, *Phys. Rev. Lett.* **80**, 5243 (1998).

[2] C. M. Bender, Making sense of non-Hermitian Hamiltonians, *Rep. Prog. Phys.* **70**, 947 (2007).

[3] R. El-Ganainy, K. G. Makris, M. Khajavikhan, Z. H. Musslimani, S. Rotter, and D. N. Christodoulides, Non-Hermitian physics and PT symmetry, *Nat. Phys.* **14**, 11 (2018).

[4] S. K. Özdemir, S. Rotter, F. Nori, and L. Yang, Parity-time symmetry and exceptional points in photonics, *Nat. Mater.* **18**, 783 (2019).

[5] M.-A. Miri and A. Alù, Exceptional points in optics and photonics, *Science* **363**, 1457 (2019).

[6] V. V. Konotop, J. Yang, and D. A. Zezyulin, Nonlinear waves in \mathcal{PT} -symmetric systems, *Rev. Mod. Phys.* **88**, 035002 (2016).

[7] L. Feng, R. El-Ganainy and L. Ge, Non-Hermitian photonics based on parity-time symmetry, *Nat. Photonics* **11**, 752 (2017).

[8] R. El-Ganainy, K. G. Makris, D. N. Christodoulides, and Z. H. Musslimani, Theory of coupled optical PT-symmetric structures, *Opt. Lett.* **32**, 2632 (2007).

[9] A. Guo, G. J. Salamo, D. Duchesne, R. Morandotti, M. Volatier-Ravat, V. Aimez, G. A. Siviloglou, and D. N. Christodoulides, Observation of \mathcal{PT} -Symmetry Breaking in Complex Optical Potentials, *Phys. Rev. Lett.* **103**, 093902 (2009).

[10] C. E. Rüter, K. G. Makris, R. El-Ganainy, D. N. Christodoulides, M. Segev, and D. Kip, Observation of parity-time symmetry in optics, *Nat. Phys.* **6**, 192 (2010).

[11] B. Peng, S. K. Özdemir, F. Lei, F. Monifi, M. Giannfreda, G. L. Long, S. Fan, F. Nori, C. M. Bender, and L. Yang, Parity-time-symmetric whispering-gallery microcavities, *Nat. Phys.* **10**, 394 (2014).

[12] C. Hang, G. Huang, and V. V. Konotop, \mathcal{PT} Symmetry with a System of Three-Level Atoms, *Phys. Rev. Lett.* **110**, 083604 (2013).

[13] Z. Zhang, Y. Zhang, J. Sheng, L. Yang, M.-A. Miri, D. N. Christodoulides, B. He, Y. Zhang, and M. Xiao, Observation of Parity-Time Symmetry in Optically Induced Atomic Lattices, *Phys. Rev. Lett.* **117**, 123601 (2016).

[14] J. Schindler, A. Li, M. C. Zheng, F. M. Ellis, and T. Kottos, Experimental study of active LRC circuits with \mathcal{PT} symmetries, *Phys. Rev. A* **84**, 040101 (2011).

[15] R. Fleury, D. Sounas, and A. Alù, An invisible acoustic sensor based on parity-time symmetry, *Nat. Commun.* **6**, 5905 (2015).

[16] X. Zhu, H. Ramezani, C. Shi, J. Zhu, and X. Zhang, \mathcal{PT} -Symmetric Acoustics, *Phys. Rev. X* **4**, 031042 (2014).

[17] L. Feng, Z. J. Wong, R.-M. Ma, Y. Wang, and X. Zhang, Single-mode laser by parity-time symmetry breaking, *Science* **346**, 972 (2014).

[18] H. Hodaei, M.-A. Miri, M. Heinrich, D. N. Christodoulides, and M. Khajavikhan, Parity-time-symmetric microring lasers, *Science* **346**, 975 (2014).

[19] J. Wiersig, Enhancing the Sensitivity of Frequency and Energy Splitting Detection by Using Exceptional Points: Application to Microcavity Sensors for Single-Particle Detection, *Phys. Rev. Lett.* **112**, 203901 (2014).

[20] Z.-P. Liu, J. Zhang, S. K. Özdemir, B. Peng, H. Jing, X.-Y. Lü, C.-W. Li, L. Yang, F. Nori, and Y.-X. Liu, Metrology with \mathcal{PT} -Symmetric Cavities: Enhanced Sensitivity near the \mathcal{PT} -Phase Transition, *Phys. Rev. Lett.* **117**, 110802 (2016).

[21] Y. Choi, C. Hahn, J. W. Yoon, S. H. Song, and P. Berini, Extremely broadband, on-chip optical nonreciprocity enabled by mimicking nonlinear anti-adiabatic quantum jumps near exceptional points, *Nat. Commun.* **8**, 14154 (2017).

[22] M. Zhang, W. Sweeney, C. W. Hsu, L. Yang, A. D. Stone, and L. Jiang, Quantum Noise Theory of Exceptional Point Amplifying Sensors, *Phys. Rev. Lett.* **123**, 180501 (2019).

[23] Y. Chu, Y. Liu, H. Liu, and J. Cai, Quantum Sensing with a Single-Qubit Pseudo-Hermitian System, *Phys. Rev. Lett.* **124**, 020501 (2020).

[24] M. Naghiloo, M. Abbasi, Y. N. Joglekar, and K. W. Murch, Quantum state tomography across the exceptional point in a single dissipative qubit, *Nat. Phys.* **15**, 1232 (2019).

[25] Y. Wu, et al. Observation of parity-time symmetry breaking in a single-spin system, *Science* **364**, 878 (2019).

[26] Yu, S. et al. Experimental Investigation of Quantum PT-Enhanced Sensor. *Phys. Rev. Lett.* **125**, 240506 (2020).

[27] S. Scheel and A. Szameit, PT-symmetric photonic quantum systems with gain and loss do not exist, *Europhysics Letters*

Lett. **122**, 34001 (2018).

[28] L. Ge and H. E. Türeci, Antisymmetric \mathcal{PT} -photonic structures with balanced positive- and negative-index materials, *Phys. Rev. A* **88**, 053810 (2013).

[29] P. Peng, W. Cao, C. Shen, W. Qu, J. Wen, L. Jiang, and Y. Xiao, Anti-parity-time symmetry with flying atoms, *Nat. Phys.* **12**, 1139 (2016).

[30] J.-H. Wu, M. Artoni, and G. C. La Rocca, Non-Hermitian Degeneracies and Unidirectional Reflectionless Atomic Lattices, *Phys. Rev. Lett.* **113**, 123004 (2014).

[31] F. Yang, Y.-C. Liu, and L. You, Anti- \mathcal{PT} symmetry in dissipatively coupled optical systems, *Phys. Rev. A* **96**, 053845 (2017).

[32] V. V. Konotop and D. A. Zezyulin, Odd-Time Reversal \mathcal{PT} Symmetry Induced by an Anti- \mathcal{PT} -Symmetric Medium, *Phys. Rev. Lett.* **120**, 123902 (2018).

[33] X.-L. Zhang, S. Wang, B. Hou, and C. T. Chan, Dynamically Encircling Exceptional Points: In situ Control of Encircling Loops and the Role of the Starting Point, *Phys. Rev. X* **8**, 021066 (2018).

[34] Y. Li, Y.-G. Peng, L. Han, M.-A. Miri, W. Li, M. Xiao, X.-F. Zhu, J. Zhao, A. Alù, S. Fan, and C.-W. Qiu, Anti-parity-time symmetry in diffusive systems, *Science* **364**, 170 (2018).

[35] Y. Jiang, Y. Mei, Y. Zuo, Y. Zhai, Jensen Li, J. Wen, and S. Du, Anti-Parity-Time Symmetric Optical Four-Wave Mixing in Cold Atoms, *Phys. Rev. Lett.* **123**, 193604 (2019).

[36] M.-A. Miri and A. Alù, Nonlinearity-induced PT-symmetry without material gain, *New J. Phys.* **18**, 065001 (2016).

[37] S. L. Braunstein and P. van Loock, Quantum information with continuous variables, *Rev. Mod. Phys.* **77**, 513 (2005).

[38] A. I. Lvovsky, Squeezed light, *Photon. Sci. Found., Technol. Appl.* **1**, 121 (2015).

[39] V. Giovannetti, S. Lloyd, and L. Maccone, Advances in quantum metrology, *Nat. Photon.* **5**, 222 (2011).

[40] L. Pezzè, A. Smerzi, M. K. Oberthaler, R. Schmied, and P. Treutlein, Quantum metrology with nonclassical states of atomic ensembles, *Rev. Mod. Phys.* **90**, 035005 (2018).

[41] See Supplementary Materials for more information about the squeezing properties, quantum Fisher information, and implementation with quantum optics and BEC.

[42] M. Tsang, Quantum transition-edge detectors, *Phys. Rev. A* **88**, 021801 (2013).

[43] M. Skotiniotis, P. Sekatski, and W. Dür, Quantum metrology for the Ising Hamiltonian with transverse magnetic field, *New J. Phys.* **17**, 073032 (2015).

[44] K. Macieszczak, M. Guță, I. Lesanovsky, and J. P. Garrahan, Dynamical phase transitions as a resource for quantum enhanced metrology, *Phys. Rev. A* **93**, 022103 (2016).

[45] Y. Chu, S. Zhang, B. Yu, and J. Cai, Dynamic Framework for Criticality-Enhanced Quantum Sensing, *Phys. Rev. Lett.* **126**, 010502 (2021).

[46] L. Garbe, M. Bina, A. Keller, M. G. A. Paris, and S. Felicetti, Critical Quantum Metrology with a Finite-Component Quantum Phase Transition, *Phys. Rev. Lett.* **124**, 120504 (2020).

[47] M. M. Rams, P. Sierant, O. Dutta, P. Horodecki, and J. Zakrzewski, At the Limits of Criticality-Based Quantum Metrology: Apparent Super-Heisenberg Scaling Revisited, *Phys. Rev. X* **8**, 021022 (2018).

[48] J. Wiersig, Review of exceptional point-based sensors, *Photon. Res.* **8**, 1457 (2020).

[49] S. E. Harris, M. K. Oshman, and R. L. Byer, Observation of Tunable Optical Parametric Fluorescence, *Phys. Rev. Lett.* **18**, 732 (1967).

[50] D. N. Klyshko, A. N. Penin, and B. F. Polkovnikov, Parametric Luminescence and Light Scattering by Polaritons, *JETP Lett.* **11**, 05 (1970).

[51] S. Du, J. Wen, and M. H. Rubin, Narrowband biphoton generation near atomic resonance, *J. Opt. Soc. Am. B* **25**, C98 (2008).

[52] L. Zhao, Y. Su, and S. Du, Narrowband biphoton generation in the group delay regime, *Phys. Rev. A* **93**, 033815 (2016).

[53] O. Morizot, Y. Colombe, V. Lorent, H. Perrin, and B. M. Garraway, Ring trap for ultracold atoms, *Phys. Rev. A* **74**, 023617 (2006).

[54] S. Eckel, J. G. Lee, F. Jendrzejewski, N. Murray, C. W. Clark, C. J. Lobb, W. D. Phillips, M. Edwards, and G. K. Campbell, Hysteresis in a quantized superfluid atomtronic circuit, *Nature* **506**, 200 (2014).

[55] A. Griffin, Conserving and gapless approximations for an inhomogeneous Bose gas at finite temperatures, *Phys. Rev. B* **53**, 9341 (1996).

[56] R. Ozeri, N. Katz, J. Steinhauer, and N. Davidson, Colloquium: Bulk Bogoliubov excitations in a Bose-Einstein condensate, *Rev. Mod. Phys.* **77**, 187 (2005).

[57] V. A. Yurovsky, Quantum effects on dynamics of instabilities in Bose-Einstein condensates, *Phys. Rev. A* **65**, 033605 (2002).

[58] E. A. Calzetta and B. L. Hu, Bose-Einstein condensate collapse and dynamical squeezing of vacuum fluctuations, *Phys. Rev. A* **68**, 043625 (2003).

[59] H. Hodaei, A. U. Hassan, S. Wittek, H. Garcia-Gracia, R. El-Ganainy, D. N. Christodoulides, and M. Khajavikhan, Enhanced sensitivity at higher-order exceptional points, *Nature* **548**, 187 (2017).

[60] S. Wang, B. Hou, W. Lu, Y. Chen, Z. Q. Zhang, and C. T. Chan, Arbitrary order exceptional point induced by photonic spin-orbit interaction in coupled resonators, *Nat. Commun.* **10**, 832 (2019).

SUPPLEMENTARY MATERIALS

S1. Two-mode squeezing

The \mathcal{APT} -symmetric matrix H is non-Hermitian, thus has biorthogonal left and right eigenstates, $H|R_{\pm}\rangle = \lambda_{\pm}|R_{\pm}\rangle$ and $H^{\dagger}|L_{\pm}\rangle = \lambda_{\pm}^*|L_{\pm}\rangle$. In the pseudo- \mathcal{APT} -broken region $|\kappa| < |\delta|$, the eigenvalues $\lambda_{\pm} = \pm\sqrt{\delta^2 - \kappa^2}$, with eigenstates $|R_{\pm}\rangle = \frac{i\kappa}{2\lambda_{\pm}}(\frac{\delta \pm \sqrt{\delta^2 - \kappa^2}}{i\kappa}, 1)^T$, $|L_{\pm}\rangle = (1, \frac{\delta \mp \sqrt{\delta^2 - \kappa^2}}{i\kappa})^T$. In the pseudo- \mathcal{APT} -symmetric region $|\kappa| > |\delta|$, $\lambda_{\pm} = \pm i\sqrt{\kappa^2 - \delta^2}$ with $|R_{\pm}\rangle = \frac{i\kappa}{2\lambda_{\pm}}(\frac{\delta \pm i\sqrt{\kappa^2 - \delta^2}}{i\kappa}, 1)^T$, $|L_{\pm}\rangle = (1, \frac{\delta \pm i\sqrt{\kappa^2 - \delta^2}}{i\kappa})^T$. We have two eigenmodes $\hat{b}_+ \propto \langle L_+ | \vec{a} \rangle$ and $\hat{b}_-^{\dagger} \propto \langle L_- | \vec{a} \rangle$ with $|\vec{a}\rangle = (\hat{a}_1, \hat{a}_2^{\dagger})^T$. We project the operators onto the eigenmodes, then the field operators at time t become

$$\begin{pmatrix} \hat{a}_1(t) \\ \hat{a}_2^{\dagger}(t) \end{pmatrix} = \begin{pmatrix} A & B \\ B^* & A^* \end{pmatrix} \begin{pmatrix} \hat{a}_1(0) \\ \hat{a}_2^{\dagger}(0) \end{pmatrix} \quad (\text{S1})$$

with the transfer matrix

$$\begin{pmatrix} A & B \\ B^* & A^* \end{pmatrix} = \sum_{s=\pm} |R_s\rangle e^{-i\lambda_s t} \langle L_s|, \quad (\text{S2})$$

where

$$A = \sum_{s=\pm} \frac{(\lambda_s - \delta)e^{i\lambda_s t}}{2\lambda_s} \quad (\text{S3})$$

$$B = \sum_{s=\pm} \frac{\kappa e^{i\lambda_s t}}{2i\lambda_s}. \quad (\text{S4})$$

At the EP $\kappa = \pm\delta$, the two eigenmodes coalesce to a single mode $\sim \hat{a}_1 \pm i\hat{a}_2^{\dagger}$, which satisfies $i\partial_t[\hat{a}_1(t) \pm i\hat{a}_2^{\dagger}(t)] = 2\delta[\hat{a}_1(0) \mp i\hat{a}_2^{\dagger}(0)]$ and depends on its time-independent orthogonal mode $\sim \hat{a}_1 \mp i\hat{a}_2^{\dagger}$. Therefore, we have the solution $A = 1 - i\delta t$, $B = \kappa t$. We can define the quadrature operators $\hat{X}_j(\varphi, t) = [e^{-i\varphi}\hat{a}_j(t) + h.c.]/2$ and $\hat{P}_j(\varphi, t) = [e^{-i\varphi}\hat{a}_j(t) - h.c.]/2i$. It can be shown that $\hat{X}_1(\varphi_+, t) \pm \hat{X}_2(\varphi_+, t) = S^{\pm 1}[\hat{X}_1(\varphi_-, 0) \pm \hat{X}_2(\varphi_-, 0)]$ and $\hat{P}_1(\varphi_+, t) \mp \hat{P}_2(\varphi_+, t) = S^{\pm 1}[\hat{P}_1(\varphi_-, 0) \mp \hat{P}_2(\varphi_-, 0)]$, with the squeezing factor $S = A_0 + B_0 \geq 1$ (with $A_0 = |A|$, $B_0 = |B|$) and the angles $\varphi_{\pm} = (\text{Arg}[B] \pm \text{Arg}[A])/2$. The oscillation behavior of S (as well as A and B) in the pseudo- \mathcal{APT} -broken region is due to the interference between two eigenmodes.

We have focused on the dynamics of the system in the main text. To see how the quantum pseudo- \mathcal{APT} symmetry is related with the ground state of the system, we write down the second-quantized Hamiltonian $\mathcal{H} = \delta \left[\hat{a}_1^{\dagger}\hat{a}_1 + \hat{a}_2^{\dagger}\hat{a}_2 \right] + i\kappa \left[\hat{a}_1^{\dagger}\hat{a}_2^{\dagger} - \hat{a}_1\hat{a}_2 \right]$. In the pseudo- \mathcal{APT} -broken region, the two eigenmodes read $\hat{b}_+ = \frac{\kappa}{\sqrt{2\lambda_0\delta-2\lambda_0^2}}\langle L_+ | \vec{a} \rangle$ and $\hat{b}_-^{\dagger} = \frac{\kappa}{\sqrt{2\lambda_0\delta+2\lambda_0^2}}\langle L_- | \vec{a} \rangle$. We have $\mathcal{H} = \lambda_0(\hat{b}_+^{\dagger}\hat{b}_+ + \hat{b}_-^{\dagger}\hat{b}_-)$ and \hat{b}_{\pm} satisfy the bosonic commutation relation. The ground state satisfy $\hat{b}_{\pm}|GS\rangle = 0$, which is a two-mode squeezed state in the $\hat{a}_{1,2}$ basis, *i.e.*, $|GS\rangle = \sum_n \sqrt{1-|q|^2}q^n|n,n\rangle$ with $q = i\frac{\delta-\lambda_0}{\kappa}$ and $|n,n\rangle$ the Fock state in $\hat{a}_{1,2}$ basis. In the pseudo- \mathcal{APT} -symmetric region, the two eigenmodes no longer satisfy bosonic commutation relation, therefore the second-quantized Hamiltonian can not be diagonalized and has no well defined ground state. The system is always dynamically unstable.

Recall that the squeezing factor S is defined based on the dynamical evolution of the field operators (*i.e.*, $\hat{X}_1(\varphi_+, t) \pm \hat{X}_2(\varphi_+, t) = S^{\pm 1}[\hat{X}_1(\varphi_-, 0) \pm \hat{X}_2(\varphi_-, 0)]$), therefore, S is independent from the initial state. However, the variance of $\hat{X}_1(\varphi, t) \pm \hat{X}_2(\varphi, t)$ does depend on the initial state. If we start from the state $|GS\rangle$, then the variance of $\hat{X}_1(\varphi, t) \pm \hat{X}_2(\varphi, t)$ should not change with time for all φ , since $|GS\rangle$ is the ground state of \mathcal{H} and thus $|GS(t)\rangle = |GS(t=0)\rangle$. On the other hand, the dynamics of the field operator in Heisenberg picture give $\hat{X}_1(\varphi_+, t) \pm \hat{X}_2(\varphi_+, t) = S^{\pm 1}[\hat{X}_1(\varphi_-, 0) \pm \hat{X}_2(\varphi_-, 0)]$, which indicate that the two-mode variance along φ_+ at time t is relatively squeezed with respect to the two-mode variance along φ_- at time 0. This means that the two-mode variance along φ_+ is $S^{\pm 2}$ times of the two-mode variance along φ_- for an initial state $|GS\rangle$ whose two-mode variance is time-independent. It can be shown that $|GS\rangle$, a two-mode squeezed state, does satisfy the above relation.

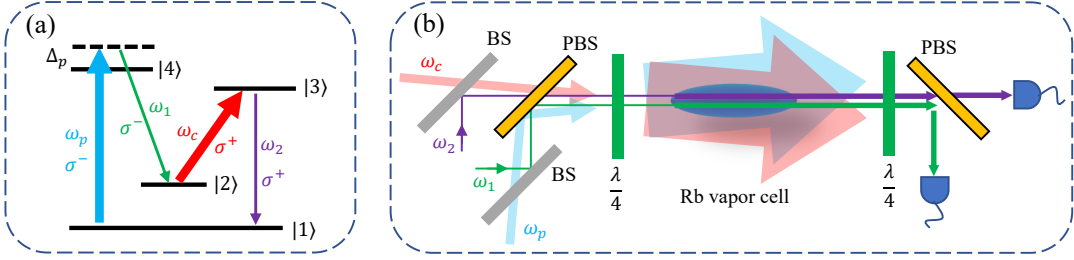


FIG. S1: Experimental realization based on nonlinear optics. (a) ⁸⁵Rb atomic energy-level diagram: $|1\rangle = |5S_{1/2}, F = 2\rangle$, $|2\rangle = |5S_{1/2}, F = 3\rangle$, $|3\rangle = |5P_{1/2}, F = 3\rangle$, $|4\rangle = |5P_{3/2}, F = 3\rangle$. (b) Schematic of the experimental setup and geometrical arrangement on four interacting fields. BS and PBS represent the beam splitter and polarized beam splitter.

S2. Quantum Fisher information

We focus on the initial coherent state $|\psi_0\rangle = |\alpha_1, \alpha_2\rangle$, and the final state reads $|\psi(t)\rangle = e^{-i\mathcal{H}t}|\psi_0\rangle$ with the second-quantized Hamiltonian $\mathcal{H} = \delta [\hat{a}_1^\dagger \hat{a}_1 + \hat{a}_2^\dagger \hat{a}_2] + i\kappa [\hat{a}_1^\dagger \hat{a}_2^\dagger - \hat{a}_1 \hat{a}_2]$. We write $|\psi_0\rangle = \hat{D}_1(\alpha_1) \hat{D}_2(\alpha_2) |0, 0\rangle$ with displacement operators $\hat{D}_j(\alpha_j) = e^{\alpha_j \hat{a}_j^\dagger - h.c.}$ and vacuum state $|0, 0\rangle$. Now we are working in the Schrödinger picture and the time-independent field operators are $\hat{a}_j = \hat{a}_j(0)$. Then we have $|\psi(t)\rangle = \hat{D}_1(\alpha'_1) \hat{D}_2(\alpha'_2) \sum_n \sqrt{1 - |q|^2} q^n |n, n\rangle$, with $\alpha'_j = A\alpha_j + B\alpha_{\bar{j}}$, $q = \frac{B}{A^*}$ and $|n, n\rangle$ the Fock state. In particular, $|\psi(t)\rangle = [e^{-i\mathcal{H}t} \hat{D}_1(\alpha_1) \hat{D}_2(\alpha_2) e^{i\mathcal{H}t}] |0, 0\rangle$. Using $e^{-i\mathcal{H}t} \hat{a}_j e^{i\mathcal{H}t} = A(-t) \hat{a}_j + B(-t) \hat{a}_{\bar{j}}^\dagger$, $A(-t) = A^*(t)$ and $B(-t) = -B(t)$, we obtain $[e^{-i\mathcal{H}t} \hat{D}_1(\alpha_1) \hat{D}_2(\alpha_2) e^{i\mathcal{H}t}] = \hat{D}_1(\alpha'_1) \hat{D}_2(\alpha'_2)$. From $\hat{a}_j |0, 0\rangle = 0$, we have $[e^{-i\mathcal{H}t} \hat{a}_j e^{i\mathcal{H}t}] e^{-i\mathcal{H}t} |0, 0\rangle = [A^* \hat{a}_j - B \hat{a}_{\bar{j}}^\dagger] e^{-i\mathcal{H}t} |0, 0\rangle = 0$, thus $e^{-i\mathcal{H}t} |0, 0\rangle = \sqrt{1 - |q|^2} \sum_n q^n |n, n\rangle$, which is a two-mode squeezed vacuum state.

The quantum Fisher information is calculated as $F_\kappa = 4\langle \partial_\kappa \psi(t) | \partial_\kappa \psi(t) \rangle - 4|\langle \partial_\kappa \psi(t) | \psi(t) \rangle|^2$ [2]. We can obtain the expression given by Eq. (7) in the main text after some algebraic manipulations.

S3. Experimental consideration

Nonlinear optics.—Our model can be realized by multi-wave mixing processes in nonlinear optical medium. Here we give more details about the experimental scheme based on four-wave mixing (the scheme based on three-wave mixing is similar). We consider the same setup as in [1], with ⁸⁵Rb atomic ensemble (prepared in ground state $|1\rangle$) as the nonlinear medium. The atomic energy-level diagram, geometrical arrangement on four interacting fields and schematic of the experimental setup are shown in Fig. S1. A pump laser (ω_p) is blue detuned by Δ_p from the atomic transition $|1\rangle \rightarrow |4\rangle$ and a weak Stokes field (ω_1) follows $|4\rangle \rightarrow |2\rangle$. Another strong coupling laser (ω_c) is on resonance at $|2\rangle \rightarrow |3\rangle$ and the weak anti-Stokes field (ω_2) drives the transition $|3\rangle \rightarrow |1\rangle$. We consider resonant mixing with energy conservation $\omega_p + \omega_c = \omega_1 + \omega_2$. The coupled equations are

$$i\partial_z \begin{pmatrix} \hat{a}_1 \\ \hat{a}_2^\dagger \end{pmatrix} = \begin{pmatrix} -\Delta k/2 & -\tilde{\kappa} \\ \tilde{\kappa} & \Delta k/2 \end{pmatrix} \begin{pmatrix} \hat{a}_1 \\ \hat{a}_2^\dagger \end{pmatrix}. \quad (\text{S5})$$

Here $\Delta k = (\mathbf{k}_1 + \mathbf{k}_2 - \mathbf{k}_p - \mathbf{k}_c) \cdot \hat{\mathbf{z}}$ is the phase mismatch with \mathbf{k}_j the corresponding wave vector and $\hat{\mathbf{z}}$ the unit vector along propagation direction z , which can be tuned by slightly changing the propagation direction of the pumping or coupling beam. $\tilde{\kappa}$ denotes the real nonlinear coupling coefficient. With a proper gauge choice $\hat{a}_2^\dagger \rightarrow \hat{a}_2^\dagger e^{i\pi/2}$, we obtain

$$i\partial_z \begin{pmatrix} \hat{a}_1 \\ \hat{a}_2^\dagger \end{pmatrix} = \begin{pmatrix} \delta & i\kappa \\ i\kappa & -\delta \end{pmatrix} \begin{pmatrix} \hat{a}_1 \\ \hat{a}_2^\dagger \end{pmatrix} = H \begin{pmatrix} \hat{a}_1 \\ \hat{a}_2^\dagger \end{pmatrix}, \quad (\text{S6})$$

with $\delta = -\Delta k/2$ and $\kappa = -\tilde{\kappa}$. For the quantum sensing, we can tune Δk to the work points satisfying $\lambda_0 L = n\pi$ with $z = L$ the length of the nonlinear medium. The initial state can be obtained by injecting weak input coherent fields in \hat{a}_j (see Fig. S1), and the measurement is realized by standard homodyne detection.

Ultra-cold atoms.—We can substitute the expansion of the BEC field operator

$$\hat{\Psi}(\theta, t) = e^{-i\mu t - i\pi/4} \Phi(t) + e^{-i\mu t} \sum_{n \neq 0} \hat{\psi}_n(t) \frac{e^{in\theta}}{\sqrt{2\pi}}, \quad (\text{S7})$$

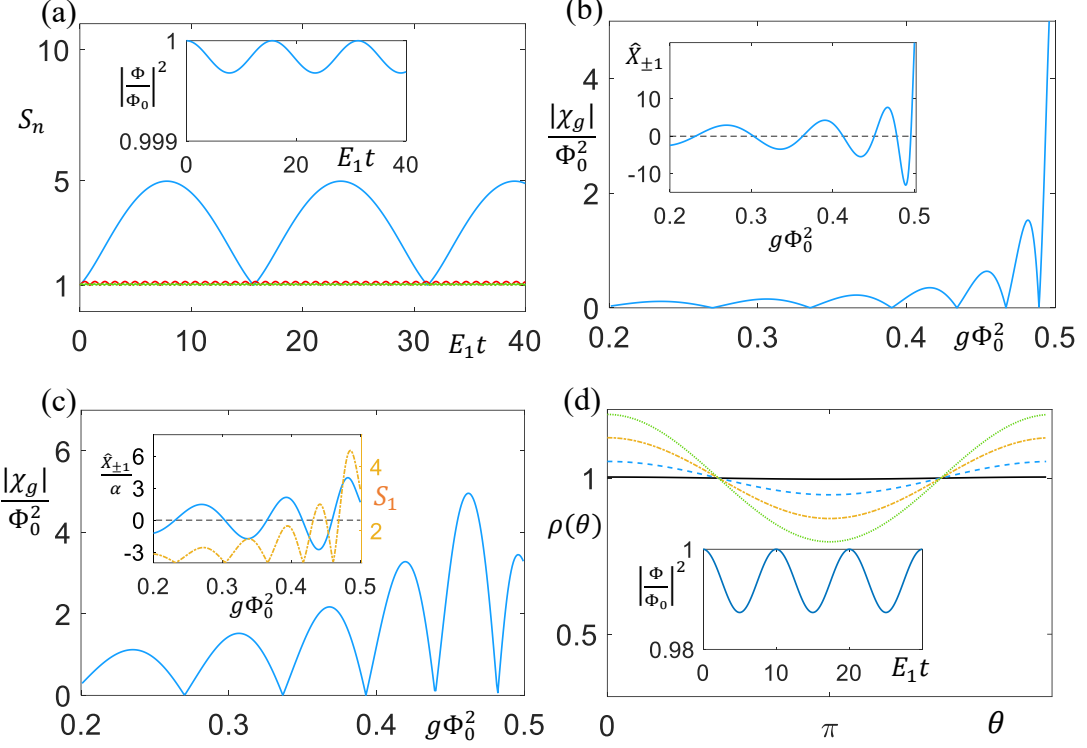


FIG. S2: Sensing based on atomic BEC trapped in a ring. (a) The squeezing factors S_n as functions of evolution time for fields $\hat{\psi}_{\pm n}$ with $g\Phi_0^2 = 0.48E_1$ and $\alpha = 2$. A larger n has a weaker squeezing factor. $n = 1, 2, 3$ are shown. Inset shows how $\Phi(t)$ changes with time. (b) and (c) The susceptibility (in unit of 10^3) as a function of $g\Phi_0^2$ at time $E_1 t = 30$ for $\alpha = 2$ and $\alpha = 20$. Inset of (b) shows the corresponding quadrature. Inset of (c) shows the corresponding quadrature (solid line) and squeezing factor (dash-dotted line). (d) Density modulation along azimuthal angle θ for $E_1 t = 30$ and $\alpha = 20$. The solid, dashed, dash-dotted and dotted lines correspond to $g\Phi_0^2 = 0.46E_1, 0.462E_1, 0.465E_1, 0.468E_1$, respectively, and the corresponding quadratures and visibilities are $\langle \hat{X}_{\pm 1} \rangle = 4.41, 14.3, 29.1, 43.2$ and $v = 0.3\%, 5.3\%, 12.9\%, 20.4\%$. Inset shows the condensed atom number during the evolution for $g\Phi_0^2 = 0.46E_1$ and $\alpha = 20$.

into the nonlinear Schrödinger equation

$$i\hbar\partial_t \hat{\Psi}(\theta, t) = \left[\frac{\hat{p}^2}{2m} - g\hat{\Psi}(\theta, t)^\dagger \hat{\Psi}(\theta, t) \right] \hat{\Psi}(\theta, t), \quad (\text{S8})$$

which gives the Hartree-Fock Bogoliubov equation

$$i\partial_t \Phi = -i\frac{g}{2\pi} \sum_n \langle \hat{\psi}_n \hat{\psi}_{-n} \rangle \Phi^* - \frac{g}{2\pi} \sum_n \langle \hat{\psi}_n^\dagger \hat{\psi}_n \rangle \Phi, \quad (\text{S9})$$

$$i\partial_t \begin{pmatrix} \hat{\psi}_n \\ \hat{\psi}_{-n}^\dagger \end{pmatrix} = \begin{pmatrix} n^2 E_1 - g|\Phi|^2 & ig\Phi^2 \\ ig(\Phi^*)^2 & -(n^2 E_1 - g|\Phi|^2) \end{pmatrix} \begin{pmatrix} \hat{\psi}_n \\ \hat{\psi}_{-n}^\dagger \end{pmatrix} \quad (\text{S10})$$

In the stable pseudo- \mathcal{APT} -broken region, excitations are weak and $\sum_n \langle \hat{\psi}_n \hat{\psi}_{-n} \rangle$ and $\sum_n \langle \hat{\psi}_n^\dagger \hat{\psi}_n \rangle$ are much smaller than Φ^2 , therefore Φ is hardly affected by the excitations.

For the quantum sensing, we can first prepare the BEC to its ground state with $g \simeq 0$. The initial coherent state for $n = \pm 1$ can be generated by the Raman process with Laguerre-Gaussian beams carrying ± 1 orbital angular momentum. Then we increase g to the working point near the EP (*i.e.*, $2g|\Phi|^2 = E_1$). For example, we can tune g using Feshbach resonance, which in turn can be used to measure the magnetic field with ultra-high precision. The sensor operates in the pseudo- \mathcal{APT} -broken region which ensures the dynamical stability of the BEC. The squeezing and excitation number for $n > 1$ are negligible since δ increases quadratically with n . Moreover, the excitation number for $n = 1$ is generally much smaller than the number of BEC atoms, so that Φ is hardly affected during the evolution, which is confirmed by our numerical simulation. The performance of the sensor (Fig. S2) is very similar as that shown in Fig. 2 in the main text. For the measurement scheme, one can detect the density $\langle \hat{\Psi}^\dagger(\theta, t) \hat{\Psi}(\theta, t) \rangle \simeq$

$\Phi^2 + \frac{2\Phi}{\sqrt{2\pi}} \sum_{n \neq 0} \langle \hat{X}_n(\varphi, t) \cos(n\theta) - \hat{P}_n(\varphi, t) \sin(n\theta) \rangle$ with $\varphi = -\pi/4$ and \hat{X}_n, \hat{P}_n the corresponding quadrature operators of $\hat{\psi}_n$. Notice that only $\langle \hat{X}_{\pm 1}(\varphi, t) \rangle$ and $\langle \hat{P}_{\pm 1}(\varphi, t) \rangle$ are nonzero (since the initial excitations are prepared on $n = \pm 1$) and they show divergent susceptibility with respect to g or E_1 .

In the following, we show the numerical simulations for the BEC-based quantum sensing. We find that ultra-high precision can be still achieved even if we consider the weak back action of the excitations on the condensate wave function, and the long-time dynamics would still be very sensitive to system parameters around the pseudo-APT transition. In Fig. S2(a), we show the squeezing factors and $|\Phi|^2$ as a function of time by solving Eq. S9 and Eq. S10 numerically. We see $|\Phi|^2$ is hardly affected even for parameters close to the exceptional point. In Fig. S2(b), we show how the quadratures $\langle \hat{X}_{\pm 1}(\varphi, t) \rangle$ and the corresponding susceptibilities change with $g|\Phi_0|^2$ (where $\Phi(0) = \Phi_0$) for $\phi = -\pi/4$. In the simulation, we have set $E_1 = 1$ as the unit, and assumed total atom number of the BEC is about $\Phi_0^2 = 10^5$, which is typical in experiments. We also consider an initial excitation state being the coherent state with amplitudes $\alpha_{+1} = \alpha_{-1} = e^{i\pi/4}\alpha$, then we have $\hat{X}_{+1}(-\pi/4, t) = \hat{X}_{-1}(-\pi/4, t)$, and $\chi_g = \partial_g \hat{X}_{+1}$. In our simulation, we have kept n up to ± 10 and checked that the results are hardly affected by increasing the cutoff of n .

For our choice with $\alpha_{+1} = \alpha_{-1} = e^{i\pi/4}\alpha$, the quadratures are $\langle \hat{X}_{\pm 1}(-\pi/4, 0) \rangle = \text{Re}[e^{i\pi/4}\alpha_{\pm 1}] = 0$ and $\langle \hat{P}_{\pm 1}(-\pi/4, 0) \rangle = \text{Im}[e^{i\pi/4}\alpha_{\pm 1}] = \alpha$. The initial density reads

$$\langle \hat{\Psi}^\dagger \hat{\Psi} \rangle \simeq \Phi_0^2 + \frac{2\Phi_0}{\sqrt{2\pi}} \sum_{n=\pm 1} \langle \hat{X}_n \rangle \cos(n\theta) - \langle \hat{P}_n \rangle \sin(n\theta) = \Phi_0^2. \quad (\text{S11})$$

There is no density modulation initially. Notice that we have $\hat{P}_{+1} = \hat{P}_{-1}$ and $\hat{X}_{+1} = \hat{X}_{-1}$ for our choice of $\alpha_{\pm 1}$, $\hat{X}_{\pm 1}$ and $\hat{P}_{\pm 1}$ correspond to density and phase modulation of the wave function, and the total density is given by $\langle \hat{\Psi}^\dagger \hat{\Psi} \rangle \simeq \Phi_0^2 + \frac{4\Phi_0}{\sqrt{2\pi}} \langle \hat{X}_1 \rangle \cos(\theta)$. This can also be seen from the initial total wave function which is $\langle \hat{\Psi} \rangle = e^{-i\pi/4} [\Phi_0 + i \frac{2\alpha}{\sqrt{2\pi}} \cos(\theta)]$. The initial excitation with nonzero $\hat{P}_{\pm 1}$ corresponds to phase modulation. We can define the normalized density as

$$\rho(\theta, t) = \frac{\langle \hat{\Psi}^\dagger \hat{\Psi} \rangle}{\Phi^2} \simeq 1 + \frac{4}{\Phi_0 \sqrt{2\pi}} \langle \hat{X}_1 \rangle \cos(\theta), \quad (\text{S12})$$

therefore, the observable $\langle \hat{X}_{\pm 1} \rangle \simeq \frac{\Phi_0 \sqrt{2\pi}}{4} v$ can be detected by density imaging with $v = \frac{\max[\rho(\theta)] - \min[\rho(\theta)]}{\max[\rho(\theta)] + \min[\rho(\theta)]}$ the visibility. Around the working point, the system nearly returns to the initial state with $\langle \hat{X}_{\pm 1} \rangle \simeq 0$ and $\langle \hat{P}_{\pm 1} \rangle \simeq \alpha$, where $\langle \hat{X}_{\pm 1} \rangle$ and thereby the density modulation is very sensitive to system parameters.

For a small α (e.g., $\alpha = 2$), the excitation number and the observable $\langle \hat{X}_{\pm 1} \rangle$ are small, therefore, the density modulation is also weak, which makes the detection hard. To obtain density modulation that is easy to detect, we need to use a larger α . On the other hand, α should not be too large so that the excitation number is much smaller than the ground-state atom number and the system can still be characterized by the Hartree-Fock Bogoliubov equation. There is a trade-off in choosing α . We find that $\alpha = 20$ can lead to density modulation with visibility $\sim 20\%$, while keeping the change in condensed atom number below 2% (as shown in Figs. S2c and S2d). Such visibility could be observed using current imaging technique, and the density modulation pattern is very sensitive to parameters (e.g., the visibility changes from 0.3% to 12.9% as $g\Phi_0^2$ changes from $0.46E_1$ to $0.465E_1$). The reason why weak excitations can lead to strong modulation is that, $\rho(\theta) = 1 + v \cos(\theta)$ correspond to a wave function $\langle \hat{\Psi} \rangle \sim \frac{1}{\sqrt{2\pi}} + \frac{v}{2\sqrt{2}} \frac{\cos(\theta)}{\sqrt{\pi}}$ (we ignored the phase modulation), and the excitation fraction [on excited state $\frac{\cos(\theta)}{\sqrt{\pi}}$] is given by $(\frac{v}{2\sqrt{2}})^2 = v^2/8$. Therefore, even for a visibility $v \sim 20\%$, the excitation fraction (or the relative change in $|\Phi(t)|^2$) is only about 0.5%. The maximum excitation fraction is reached when the quadrature $\langle \hat{X}_1 \rangle$ and also the squeezing factor S_1 reach their maximum, which is away from the working point and the corresponding susceptibility drops to 0. For $g\Phi_0^2 = 0.46E_1$ and $\alpha = 20$, the maximum excitation fraction is about 1.3% (see the inset of Fig. S2d at $E_1 t \simeq 5, 15, 25, \dots$), and the corresponding maximum visibility is about 30%.

Notice that, if we start from the exceptional point $g\Phi_0^2 = 0.5E_1$, the system will evolve back to the symmetry broken region due to the oscillation of $\Phi^2(t)$ (the oscillation is stronger for larger α), therefore, the transition at $g\Phi_0^2 = 0.5E_1$ is no longer sharp, but behaves like a crossover.

* Electronic address: Chuanwei.Zhang@utdallas.edu

† Electronic address: dusw@utdallas.edu

[1] Y. Jiang, Y. Mei, Y. Zuo, Y. Zhai, J. Li, J. Wen, and S. Du, Anti-Parity-Time Symmetric Optical Four-Wave Mixing in Cold Atoms, [Phys. Rev. Lett. **123**, 193604 \(2019\)](https://doi.org/10.1103/PhysRevLett.123.193604).

[2] L. Pezzè, A. Smerzi, M. K. Oberthaler, R. Schmied, and P. Treutlein, Quantum metrology with nonclassical states of atomic ensembles, *Rev. Mod. Phys.* **90**, 035005 (2018).
